

Wave Turbulence in Quantum Fluids

German V. Kolmakov ^{*}, Peter V. E. McClintock [†] and Sergey V. Nazarenko [‡]

^{*}Physics Department, New York City College of Technology, City University of New York, Brooklyn, NY 11201, USA, [†]Department of Physics, Lancaster University, Lancaster LA1 4YB, United Kingdom, and [‡]Mathematics Institute, University of Warwick, Coventry CV4 7AL, United Kingdom

Submitted to Proceedings of the National Academy of Sciences of the United States of America

Wave turbulence (WT) occurs in systems of strongly interacting nonlinear waves, and can lead to energy flows across length and frequency scales much like those that are well known in vortex turbulence. Typically, the energy passes through a non-dissipative inertial range until it reaches a small enough scale that viscosity becomes important and terminates the cascade by dissipating the energy as heat. Wave turbulence in quantum fluids is of particular interest, partly because revealing experiments can be performed on a laboratory scale, and partly because WT among the Kelvin waves on quantized vortices is believed to play a crucial role in the final stages of the decay of (vortex) quantum turbulence. In this short review, we provide a perspective on recent work on WT in quantum fluids, setting it in context and discussing the outlook for the next few years. We outline the theory, review briefly the experiments carried out to date using liquid H₂ and liquid ⁴He, and discuss some nonequilibrium excitonic superfluids in which WT has been predicted but not yet observed experimentally. By way of conclusion, we consider the medium- and longer-term outlook for the field.

turbulence | nonlinear waves | quantum fluids

1. Introduction

Wave turbulence (WT) (1, 2) is probably less familiar than ordinary (vortex) turbulence to most scientists, but the two sets of phenomena are actually very similar. Unlike electromagnetic waves in the vacuum, which are linear, and can therefore pass through each other unaltered, waves in a nonlinear medium interact with each other, sometimes strongly. WT manifests itself in systems of strongly-interacting nonlinear waves. They form a disordered system in which there can be non-dissipative flows of energy across the frequency and length scales, much as occur in vortex turbulence. WT arises in a wide variety of classical contexts, including e.g. surface waves on water (both gravity and capillary) (3–5), nonlinear optical systems (6, 7), sound waves in oceanic waveguides (8), shock waves in the solar atmosphere and their coupling to the Earth's magnetosphere (9), and magnetic turbulence in interstellar gases (10). There is a large and rapidly expanding literature, to which many relevant references up to mid-2010 are listed in (2). As we discuss in more detail below, WT can also occur in quantum fluids, where it exhibits some distinctive features. Experimental studies have included surface waves on liquid H₂ (11) and liquid helium (12), and second sound in superfluid ⁴He (13). Very recently, wave turbulence has been demonstrated and studied numerically in the nonequilibrium excitonic superfluids (14) that occur in semiconductors (15) including graphene (16).

In section 2 we review briefly the theory of WT, concentrating on the aspects relevant to quantum fluids. Section 3 describes the relevant experiments reported to date, and also describes a numerical experiment showing that WT can also occur in semiconductor Bose-Einstein condensates (BECs). Finally, in section 4, we conclude and consider the future for research in the area.

2. Theory of wave turbulence in quantum fluids

First of all, we would like to draw a distinction between WT and “weak turbulence”. By the former we understand a real physical phenomenon in a non-equilibrium statistical system where random interacting waves constitute the fundamental building blocks. By the

latter we mean an idealised system where all interacting waves are weak and have random phases, so that it can therefore be described by a wave kinetic equation. Thus, in real-life applications WT may not be, and seldom is, weak. Most often, WT systems include both random weak waves and strong coherent structures, with these two components interacting and exchanging energy in a WT life cycle (2).

However, weak turbulence provides a theoretical framework for WT and allows one to understand many (although not all) physical effects observed in real systems of random waves. Weak turbulence theory usually considers dispersive systems, with a couple of important exceptions being magnetohydrodynamic (MHD) turbulence and acoustic turbulence. It is based on two fundamental assumptions: that the waves are weakly nonlinear, and that they have random phases. It is further assumed that the system is infinite in the physical space and statistically homogeneous. The main outcome of the weak turbulence derivation is a wave kinetic equation describing the evolution of the wave spectrum. Depending on the system, the kinetic equation can be three-wave, four-wave or higher-order: see examples in the following sections. Besides the usual thermodynamic Rayleigh-Jeans spectra, which represent a limiting case of a general Bose-Einstein distribution, the kinetic equations often have strongly non-equilibrium steady-state solutions similar to Kolmogorov cascades in classical hydrodynamic turbulence, the so-called Kolmogorov-Zakharov (KZ) spectra.

Quantum fluids provide plenty of physical examples where WT is either a stand-alone phenomenon or a part of a large turbulent system. Besides the systems where WT was implemented and demonstrated experimentally, there are examples where the presence of WT has been hypothesized but not yet experimentally confirmed. Nonetheless it has firmly taken its niche in the theoretical description of the quantum turbulence phenomenon. The two most prominent examples here are small-scale turbulence in superfluid helium and turbulence in Bose-Einstein condensates. We will start the description of our examples with these two systems, after which we will present examples where WT was actually observed experimentally.

Wave turbulence in Bose-Einstein condensates. A detailed review of WT in BEC can be found in the book (2). Here we will restrict ourselves to a brief description of the most fundamental phenomena in BEC turbulence. Note that the theory of BEC turbulence is much more advanced than the corresponding experimental studies; the latter have only begun relatively recently (17).

The modeling of BEC turbulence starts with the Gross-Pitaevskii (a.k.a. Nonlinear Schrödinger) equation,

$$i\dot{\psi}(\mathbf{x}, t) + \nabla^2\psi(\mathbf{x}, t) - \psi(\mathbf{x}, t)|\psi(\mathbf{x}, t)|^2 = 0, \quad [1]$$

Reserved for Publication Footnotes

where ψ is a complex function called the condensate wave function. (The dot over ψ in Eq. 1 denotes differentiation with respect to time t .) In this subsection we will mostly discuss the three-dimensional case, $\mathbf{x} \in R^3$, with a brief remark about the two-dimensional (2D) case at the end of the subsection. In addition to being used to describe BEC, the Gross-Pitaevskii equation is also applied to the description of optical systems, water waves, cosmology, and superfluids. This makes it one of the most universal partial differential equations in physics. The second term describes the dispersion of the waves while the third term corresponds to mutual interactions between the waves or particles. For the sake of convenience, in this section we use Eq. 1 in its non-dimensional form; the physical meanings of the dimensional coefficients in realizations for actual physical systems are different.

Equation 1 conserves the total number of particles

$$\mathcal{N} = \int |\psi|^2 d\mathbf{x} \quad [2]$$

and the total energy

$$E = \int |\nabla\psi|^2 d\mathbf{x} + \frac{1}{2} \int |\psi|^4 d\mathbf{x}. \quad [3]$$

Let us consider a system in a double-periodic square box with side L and define the Fourier transform,

$$\hat{\psi}_{\mathbf{k}} = \frac{1}{L^2} \int_{\text{box}} \psi(\mathbf{x}) e^{-i\mathbf{k}\cdot\mathbf{x}} d\mathbf{x}, \quad [4]$$

where the wave vectors \mathbf{k} take values on a lattice,

$$\mathbf{k} = \left(\pm \frac{2\pi m_x}{L}, \pm \frac{2\pi m_y}{L}, \pm \frac{2\pi m_z}{L} \right), \quad m_x, m_y, m_z = 0, 1, 2, \dots$$

The wave spectrum is defined as follows,

$$n_{\mathbf{k}} = \frac{L^2}{(2\pi)^2} \langle |\hat{\psi}_{\mathbf{k}}|^2 \rangle, \quad [5]$$

where the brackets $\langle \dots \rangle$ denote an ensemble average. Following the standard setup of the weak turbulence approach, i.e. assuming a small nonlinearity and random phases, in an infinite box limit one can derive a four-wave kinetic equation (6):

$$\dot{n}_{\mathbf{k}} = 4\pi \int n_{\mathbf{k}_1} n_{\mathbf{k}_2} n_{\mathbf{k}_3} n_{\mathbf{k}} \left[\frac{1}{n_{\mathbf{k}}} + \frac{1}{n_{\mathbf{k}_3}} - \frac{1}{n_{\mathbf{k}_1}} - \frac{1}{n_{\mathbf{k}_2}} \right] \times \delta(\omega_{\mathbf{k}} + \omega_{\mathbf{k}_3} - \omega_{\mathbf{k}_1} - \omega_{\mathbf{k}_2}) \delta(\mathbf{k} + \mathbf{k}_3 - \mathbf{k}_1 - \mathbf{k}_2) d\mathbf{k}_1 d\mathbf{k}_2 d\mathbf{k}_3. \quad [6]$$

where

$$\omega_{\mathbf{k}} = k^2 \quad [7]$$

is the dispersion relation for the wave frequency. Equation 6 is the quasi-classical limit of a general quantum kinetic equation for non-condensed systems that holds in the case of large occupation numbers $n_{\mathbf{k}}$ (1). The kinetic equation 6 also holds in the presence of a “weak” Bose-Einstein condensate, where the condensate density is small, and hence the turbulent fluctuations are relatively large. In weakly interacting systems, this case can be realized in the vicinity of the superfluid transition where the macroscopic occupation of the $k = 0$ state is small. At temperatures much lower than the transition temperature, the condensate density is large, and the corresponding equation for the occupation numbers turns into the so-called three-wave kinetic equation (18, 19).

The KZ spectra are non-equilibrium steady state solutions of the kinetic equation 6,

$$n_{\mathbf{k}} = C k^\nu,$$

with constant dimensional pre-factors C and exponents $\nu = \nu_E = -3$ and $\nu = \nu_{\mathcal{N}} = -7/3$ for the direct energy and the inverse particle cascades respectively (6). The KZ solutions are only meaningful if they are local, i.e. when the collision integral in the

kinetic equation converges. The inverse \mathcal{N} -cascade spectrum appears to be local, whereas the direct E -cascade spectrum is log-divergent at the infrared (IR) limit (i.e. at $k \rightarrow 0$) (6). Such a log-divergence can be remedied by a log-correction to the spectrum, $n_{\mathbf{k}} \sim [\ln(k/k_f)]^{-1/3} k^{\nu_E}$, where k_f is an IR cutoff provided by the forcing scale.

In the BEC context, the dual cascade behaviour has a nice interpretation. The forward cascade of energy corresponds to the strongly non-equilibrium process of evaporative cooling. Indeed, after reaching the highest momentum states, the energy will spill out of the system over the potential barrier of the retaining magnetic trap. On the other hand, the inverse cascade of particles corresponds to the beginning of the condensation process.

After populating the lowest momentum states, the system will cease to be weakly nonlinear (20). The weak turbulence description based on the four-wave kinetic equation (6) will break down, and the system will enter a strongly nonlinear phase characterised by a gas of chaotic vortices of the hydrodynamic type. These vortices will decrease in number because of a vortex annihilation process, until they reach a final coherent state, the condensate, with only a few remaining vortices or no vortices at all (21). The remaining fluctuations on the background of the condensate will be Bogolyubov phonons which can also be described by a WT kinetic equation, but this will now be a three-wave system of weakly nonlinear acoustic waves (2, 6, 18, 19).

It is interesting that, during these final stages of evolution, the few remaining vortices in the system (if present) also exhibit wave motions which can be classified as WT (21). These are so-called Kelvin waves propagating along the quantised vortex lines. We will briefly discuss such a 1D WT in next subsection.

A brief remark is due about 2D BEC turbulence. As often in dimensions of two or less, this system is special. It exhibits no true long-range order in the infinite box limit, but there is a Berezinskii-Kosterlitz-Thouless transition to states with slowly decaying power-law correlations (22). WT theory is also very special for the 2D Gross-Pitaevskii system, e.g. there are no valid KZ spectra (23, 24). Indeed, the direct cascade spectrum exponent formally coincides with that of the thermodynamic energy equipartition state, whereas the particle flux is in the “wrong” direction in the particle cascade solution.

Equation 1 describes the dynamics of a spatially homogeneous system. If it is placed in an external trapping potential $V(\mathbf{x})$, an extra term $V(\mathbf{x})\psi(\mathbf{x}, t)$ should be added to the right-hand side of Eq. 1. In effect, the condensate density in the ground state, $|\psi(\mathbf{x})|^2$, becomes coordinate-dependent, corresponding to a non-uniform BEC. WT theory can still be used in this case, for both the weak condensate (four-wave) and the strong condensate (three-wave) cases, provided that the characteristic mean-free path of the excitation wavepackets is less than the size of the trap. In this case the kinetic equation has to be modified by replacing the partial derivative of the spectrum on the left-hand side with the time derivative along the wave packet trajectory in the coordinate-wavenumber space (2, 18). The opposite case, when the characteristic mean-free path of the excitation wavepackets is greater than the size of the trap, has been less studied. One approach to this problem lies in the expansion of the condensate wave function over a basis of exact solutions of a linearized Gross-Pitaevskii equation with the trapping potential, instead of expansion over plain waves (Eq. 4). In this case, the correlation function Eq. 5 has the meaning of the occupation number for the corresponding oscillatory mode. This approach is applied, for example, to the BEC of indirect excitons in coupled quantum wells, as detailed below.

Kelvin wave turbulence. Kelvin waves propagating on quantised vortex lines have been widely discussed in the literature as a fundamental motions responsible for cascading energy below the mean inter-vortex separation scale to much smaller scales where it can be dissipated via radiation of phonons (25). There have been significant theoretical advances in applying the WT approach to the Kelvin wave system, including obtaining KZ-type spectrum (26–28). However, the main results and conclusions of such theoretical efforts require testing and validation by both numerical and experimental means. Such tests would be especially timely considering the ongoing theoretical controversy in this area (27, 29–35).

The main experimental challenge here is related to the fact that the Kelvin wave scales are not yet accessible by direct measurement techniques. Theoretically and numerically, the main difficulty is that Kelvin waves are only part of the evolving turbulent system: they coexist with polarised vortex bundles forming a Kolmogorov-type cascade of eddies in the large-scale range (above the inter-vortex separation scale) (36); they arise from, and interact with, vortex reconnection events (37, 38). Also, in reality, Kelvin waves propagate on vortex lines which themselves are neither straight nor stationary, as assumed by the idealised WT setup. Interaction of the Kelvin waves with large-scale curvature of underlying vortex lines is likely to have an important influence on the wave spectrum evolution, and this process requires a careful future study.

Excitonic superfluids in semiconductors. Excitonic superfluid represents another remarkable example of a system where turbulence can be formed under certain conditions. An exciton is a hydrogen-like bound state of a negatively charged electron and a positively charged hole in a semiconductor (39, 40). The ground state energy of the electron-hole pair is given by the famous Bohr equation $\mathcal{E}_0 = -m_r e^4 / (\epsilon \hbar)^2$, where m_r is the reduced mass of the pair, e is the electron charge, and ϵ is the dielectric constant of the material. Below, we consider gallium arsenide (GaAs), a group III-V semiconductor, as a representative example where excitonic effects are of essential importance (39–43). For GaAs, with $\epsilon \approx 13$, $m_r \approx m_0/21$ where m_0 is the free electron mass, the resultant binding energy of the exciton $-\mathcal{E}_0 \approx 3.9$ meV is much smaller than that of a hydrogen atom. In experiments, the positive and negative charges which form the excitons are usually localized in quasi-two dimensional heterostructures; specifically, the electrons and holes are positioned in two different, neighboring, nm-thick semiconductor layers (or, quantum wells) separated by an insulating barrier (41, 42, 44–46). This arrangement results in a substantial increase of exciton lifetime, compared to having the charges in a single quantum well, because of the relatively low probability of quantum tunneling of charges through the barrier. The increased exciton lifetime allows one to reach quasi-equilibrium in the system more easily, and permits one to observe Bose-Einstein condensation of the excitons, as described below. These excitons, composed of spatially separated electrons and holes, are usually referred to as *dipolar excitons* because they carry a non-zero average electric dipole moment in the direction perpendicular to the plane of the quantum wells. In addition, the dipolar excitons can be spatially localized in the heterostructure by applying an in-plane trapping potential produced by mechanical stress (43), or an electrostatic trap (47). Trapping in the quantum wells plane permits one to avoid spreading of the excitons in the sample and hence to increase the exciton two-dimensional density thus, producing more favorable conditions for Bose-Einstein condensation.

At temperatures below $T_0 \ll |\mathcal{E}_0|/k_B \sim 44$ K, Bose-Einstein condensation occurs in the system, and the dipolar excitons form a superfluid, see (14) for review. (Here, k_B is the Boltzmann constant.) Because of the two-dimensional character of exciton motion in the quantum wells, the superfluid transition is of the Berezinskii-Kosterlitz-Thouless type mentioned above, that is, it is associated with pairing of the quantized vortices in the condensate. Over the past decade, the dynamics of the exciton superfluid has attracted much at-

ention because of the potential for using excitons as the physical basis of a new generation of integrated circuits and optical computing systems (48–52). We now briefly review the approaches that permit one to study the collective quantum dynamics in a quasi-two-dimensional excitonic system within the same methodology as was formulated above for superfluid helium and atomic Bose-Einstein condensates.

At temperature much lower than that of the superfluid transition T_0 , the dynamics of the dipolar exciton BEC is described by the generalized Gross-Pitaevskii equation

$$i\hbar\dot{\psi}(\mathbf{x}, t) = -\frac{\hbar^2}{2m_{\text{ex}}}\nabla^2\psi(\mathbf{x}, t) + V(\mathbf{x})\psi(\mathbf{x}, t) + g\psi(\mathbf{x}, t)|\psi(\mathbf{x}, t)|^2 + i\hbar\left(\hat{R} - \gamma\right)\psi(\mathbf{x}, t). \quad [8]$$

where the condensate wave function $\psi(\mathbf{x}, t)$ depends on the 2D in-plane coordinate $\mathbf{x} = (x, y)$ and time t , $m_{\text{ex}} \approx 0.22m_0$ is the exciton effective mass, $V(\mathbf{x}) = \alpha|\mathbf{x}|^2/2$ is an external trapping potential (in what follows, we will focus on effects in parabolic traps, but this is not a restriction of the approach developed), $\gamma = 1/2\tau_{\text{ex}}$ is the effective damping in the system due to exciton recombination, and $\tau_{\text{ex}} \approx 100$ ns is the exciton lifetime. The first term on the right-hand side of Eq. 8 describes the kinetic energy of excitons, whereas the third, nonlinear term corresponds to mutual scattering of the excitons in the condensate. We note that Eq. 1 is written in dimensionless units whereas we use dimensional units in Eq. 8 to show how the coefficients depend on the physical parameters of the system. Equation 8 can be reduced to the non-dimensional form (Eq. 1) by representing time and distance in natural units $t_0 = (m_{\text{ex}}/\alpha)^{1/2}$ and $\ell_0 = (\hbar^2/\alpha m_{\text{ex}})^{1/4}$. Equation 8 represents a natural generalization of the “traditional” Gross-Pitaevskii Equation 1 for systems where there is continuous pumping and decay of the particles. The last term in Eq. 8 captures the fact that the excitons can be created and can decay; in addition, an external trapping potential $V(\mathbf{x})$ is taken into account. A linear operator \hat{R} captures the exciton creation due to coupling with the external laser radiation.

For dipolar excitons the interaction strength g is a function of the exciton density; the interaction strength should therefore be determined self-consistently from the equation for the chemical potential of the whole system (15). The dependence of the interaction g on the density arises from the long-range, $\propto 1/|\mathbf{x}|^3$, character of the electric dipole-dipole interactions of the excitons in coupled quantum wells. We focus on the case of a dilute dipolar exciton gas because this corresponds to experiments with excitonic BECs (42, 43). For a high-density gas, the formation of bi-excitons or crystallization effects must be taken into account (46, 53, 54), as well as nonlinear damping related to finite-density effects (55). In the model Eq. 8, we consider the low-temperature limit where the density of thermal activated excitons above the condensate is negligible. For relatively high temperatures or very high pumping rates, the condensate density profile can be significantly distorted by scattering on a bath of non-condensed excitons that sometimes results in the formation of ring-like patterns around the excitation spot (56). In Sec. 3 (penultimate subsection) below we describe the results of numerical experiments for a nonlinear excitonic superfluid based on the solution of Eq. 8.

3. Experiments on wave turbulence in quantum fluids

From an experimental point of view, quantum fluids offer many advantages for the study of WT. In particular, they have very low (or zero) viscosity compared to conventional fluids, and they can be controlled, unlike natural systems such as the ocean or the interstellar plasma. We now consider a few quantum fluid systems in which WT has been demonstrated experimentally and investigated in detail, and two in which WT has been observed numerically but not yet experimentally.

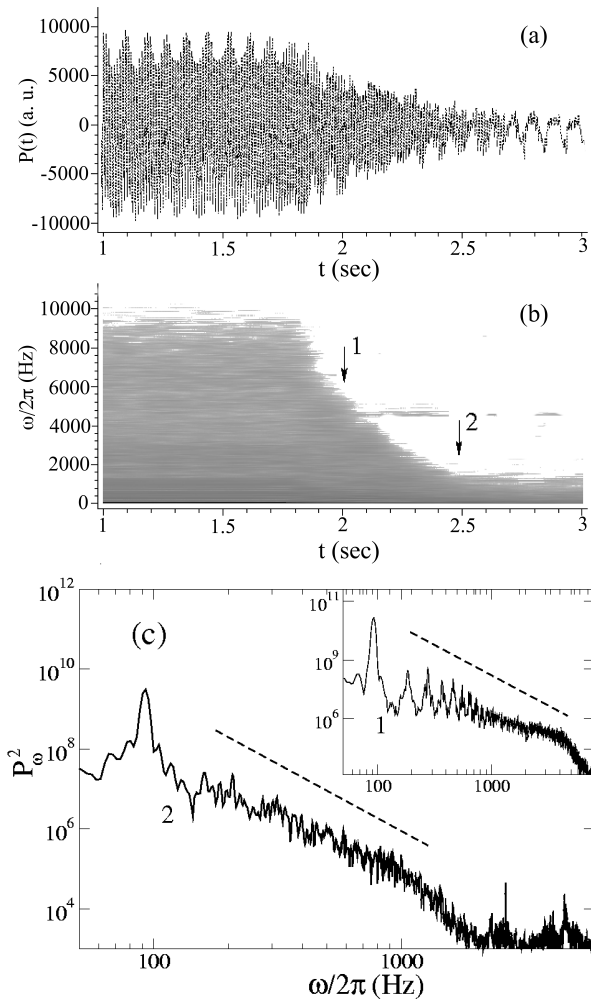


Fig. 1. Decaying turbulence of capillary waves on liquid H_2 . The measured signal $P(t)$ is proportional to the surface inclination. (a) The periodic driving force was switched off at time $t = 1.8$ s. (b) Evolution of the turbulent power spectrum during the decay, calculated over $P(t)$. Grey shading indicates frequency components in the power spectrum whose P_ω^2 exceeds the threshold 10^4 (a.u.) in the graph below. (c) Instantaneous power spectra calculated at times indicated by the arrows in (b): curve 1 in the inset corresponds to time $t = 2$ s; curve 2 corresponds to $t = 2.5$ s. The spectra shown represent an ensemble average over ten identical measurements. The dashed lines in (c) corresponds to the power-law-like dependence $P_\omega^2 \propto \omega^{-7/2}$ predicted by WT theory for capillary waves (57,58). After (11).

Atomic BEC. BECs of cold atoms can be formed in magnetic traps at extremely low temperatures $T \sim 10^2$ nK (59,60). An atomic BEC is a generic example of a degenerate quantum system whose dynamics is described by WT (18, 19). Impact on everyday life may not yet be generally appreciated, but it is worth noting that experimental work on atomic BECs has also resulted in fast progress in the development of atomic clocks, i.e. in the technology that provides International Atomic Time (IAT), the basis of the general purpose Global Positioning System (GPS) which is familiar to everyone.

In a parabolic trap, the BEC density in the ground state is well described by the parabolic Thomas-Fermi distribution, with small corrections at the edges of the atomic cloud (60). This close correspondence with Thomas-Fermi theory shows that the quantum fluctuations of the particle momenta in the BEC due to finite cloud size are negligible compared to the interaction with the external trap and the mutual interactions between the particles. If the respective curvatures of the trapping potential in all three directions are compara-

ble with each other, the condensate cloud is essentially three dimensional. However, if the curvature in one direction is much higher than the those in two other directions, the cloud has a “pancake” shape and can be considered to a first approximation as two-dimensional. Together, the direct (energy) and inverse (number of particles) cascades control the dynamics of atomic BEC formation; however, the details are different for bulk, three-dimensional, and quasi-two dimensional condensates, in agreement with the general theory sketched above.

Capillary waves on the surface of liquid H_2 . The surface of liquid H_2 offers particular advantages for the study of WT among capillary waves. It can be charged through the injection of ions into the underlying bulk liquid, and surface waves can then be excited by driving the charged surface with an alternating electric field. Furthermore, the superposition of a constant electric field can be used to counteract the effect of gravity, thus extending the capillary range to lower frequencies. The response of the surface can be measured by reflecting a laser beam from it. Full experimental details are given by Brazhnikov *et al.* (61) and in (62).

Measurements in the stationary state of steady driving (61,63) revealed the formation of WT with a Kolmogorov power law spectrum, over a wide frequency range ($10^2 - 10^4$ Hz), with a high frequency cut-off caused by the onset of viscous damping, which terminated the energy cascade (64). The spectrum is discrete in character on account of the finite radius of the pool of liquid. The scaling index of the turbulent spectrum was found to depend on the spectral content of the driving force.

Measurements of how the steady state WT decays when the driving force is suddenly switched off (11, 65) have been very revealing. The decay starts from the high frequency end of the spectrum, while most of the energy remains localised at low frequencies (Fig. 1), contrary to the original theoretical expectation based on the self-similar theory of nonstationary WT processes (1). The reason is that viscous dissipation is actually nonzero at all frequencies (even in what, for steady state driving, is the inertial regime) (66). During the decay, nonlinear wave interactions result in a rapid redistribution of energy between the frequency scales. Consequently, the whole spectrum decays together, but the top end goes down faster because of the larger viscous effects at high frequencies.

Capillary waves on the surface of liquid 4He . Experiments have also been performed (12, 67, 68) to investigate capillary waves on the surface of superfluid 4He at 1.7 K. The technique was similar to that used for hydrogen. WT with a turbulent Kolmogorov power law spectrum was observed, but there was sometimes an interesting deviation from this law near the high frequency edge of the spectrum. For steady state harmonic driving at amplitudes that were not too large, a local maximum appeared in the spectrum representing an accumulation of wave energy at that frequency. The authors attribute it (68) to an energy transfer bottleneck resulting from a detuning of the discrete surface excitations. As in the case of liquid H_2 , the form of the driving force influenced the form of the WT power spectrum.

Second sound waves in superfluid 4He . Wave turbulence among second sound waves, a form of acoustic turbulence, has been investigated in the bulk of superfluid 4He . Below its transition temperature T_λ liquid 4He behaves as though it were composed of two interpenetrating fluids, the normal and superfluid components, each of which completely fills the container. Second sound is an entropy-temperature wave corresponding to antiphase motion of the two components. Its nonlinearity coefficient α is conveniently adjustable by varying the temperature (69, 70). (The nonlinearity coefficient is introduced in a standard way through the dependence of the second sound velocity on the wave amplitude δT as $c_2 = c_{20}(1 + \alpha\delta T)$ where c_{20} is the speed of a second sound wave of infinitely small amplitude.) Thus second sound can have a nonlinearity of either sign, or even zero, and the nonlinearity can in principle be made ar-

bitrarily large as the nonlinearity coefficient diverges to $-\infty$ as T_λ is approached from below.

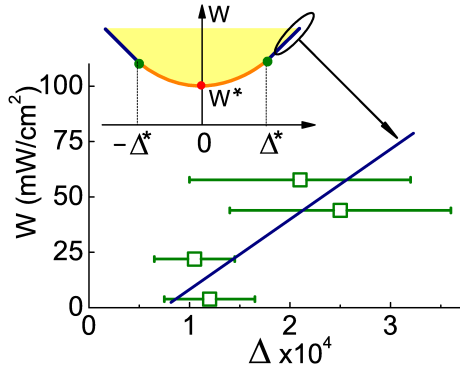


Fig. 2. Second sound turbulence: the dependence of the AC heat flux density W at which the instability develops on the dimensionless frequency detuning $\Delta = (\omega_d - \omega_n)/\omega_n$ of the driving force frequency ω_d from a cavity resonance ω_n . Numerical calculations (line) are compared with measurements (points) for driving on the 96th resonance. Horizontal bars mark the widths of the hysteretic region where second sound exists in a metastable state. Inset: bifurcation diagram showing regions of stability (unshaded) and regions of instability (yellow shaded) against the generation of subharmonics. The soft instability occurs over the (orange) line between the (green) critical points at $\pm\Delta^*$; outside them lies the hard instability; W^* is the threshold value of the instability. After (71).

The experiments involve exciting a standing wave of second sound with a heater in a cavity with a high quality Q -factor, where large amplitudes (and correspondingly strong nonlinear wave interactions) can be achieved. The temperature variations corresponding to second sound are measured with a superconducting bolometer. The results are at first sight rather similar to those from surface waves on liquid H_2 and 4He : there is a discrete WT spectrum of disordered (72) waves, and a power-law Kolmogorov-like cascade of energy towards higher frequencies (13). Under the right conditions, however, an instability against subharmonic generation can develop, leading to an inverse cascade. It involves a flux of energy towards *lower* frequencies (71). The onset of the inverse cascade as the heater power is increased is of a critical character, which can be related to the need to overcome dissipation. By direct numerical integration of the 2-fluid thermohydrodynamical equations, expanded up to quadratic terms in the wave amplitude, it was possible to account for these phenomena theoretically. A key feature of the calculation is that explicit account was taken of wave damping at all frequencies. The results are shown in Fig. 2. The main figure compares the calculated and measured values of the critical driving amplitude at which the instability develops. There is considerable hysteresis in the experimental measurements, which is consistent with the theoretical prediction of a hard instability in the relevant parameter range, as shown by the inset bifurcation diagram.

The transient behaviour of the second sound system is of particular interest. When the system is switched on, under conditions such that an inverse energy cascade is expected, the sequence of events is that: the direct cascade builds up fast, almost immediately; there is an intermediate interval within which isolated “rogue waves” (waves that are very much larger than any of their neighbours) appear (73); and finally the inverse cascade appears. The results of the observations are shown in Fig. 3. In steady state, the energy injected from the heater is shared between the forward and inverse cascades. During the build-up of the direct cascade, the initial growth of spectral amplitude follows power laws that become steeper with increasing harmonic number, behaviour that corresponds to a propagating front in frequency space (74). Each successive harmonic suffers a larger onset delay, and the data are well described by the self-similar theory.

The decay of the WT when the driving force was switched off was found to exhibit complex and interesting dynamics (75). As in the case of WT among capillary surface waves (see above), the decay started from the high frequency end of the spectrum. A windowed Fourier analysis revealed very complicated and seemingly chaotic behaviour of the individual harmonic amplitudes which has yet to be accounted for theoretically.

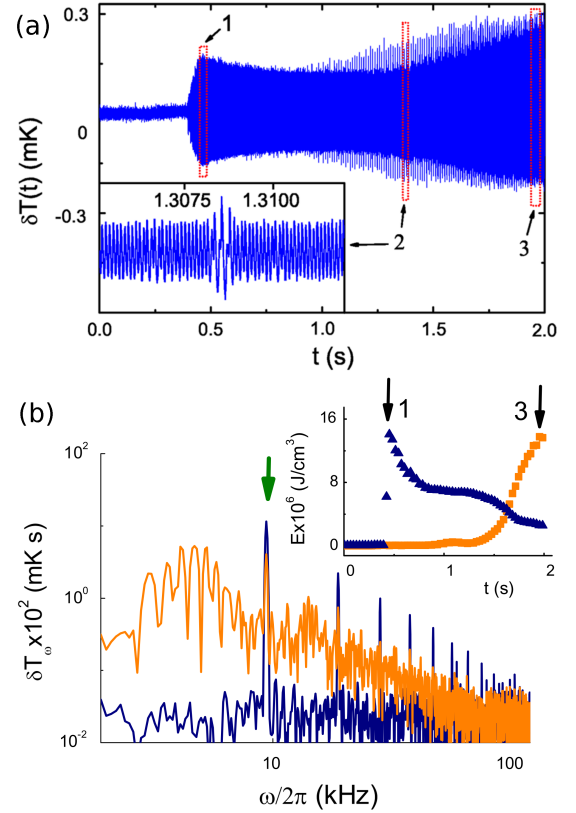


Fig. 3. (a) Transient evolution of the 2nd sound wave amplitude δT after a step-like shift of the driving frequency to the 96th resonance at time $t = 0.397$ s. Formation of isolated “rogue” waves is clearly evident. Inset: Example of a rogue wave, enlarged from frame 2. (b) Instantaneous spectra in frames 1 and 3 of figure (a). The lower (blue) spectrum, for frame 1, shows the direct cascade only; the upper (orange) spectrum, for frame 3, shows both the direct and inverse cascades. The green arrow indicates the fundamental peak at the driving frequency. Inset: Evolution of the wave energy in the low-frequency and high-frequency domains is shown by the orange squares and blue triangles respectively; black arrows mark the positions of frames 1 and 3. After (71).

Coupled first sound-second sound waves in superfluid 4He . At temperatures close to the superfluid transition temperature T_λ or at elevated pressures, second sound waves in superfluid 4He become coupled to first sound, i.e. to the ordinary pressure (density) waves (76, 77). In this case, mutual transformations between the first and second sound waves due to nonlinearity provide an additional channel for energy propagation and relaxation in the system. In superfluid helium, the characteristic relaxation time for first sound, τ_1 , is much shorter than that for second sound, τ_2 , namely $\tau_1/\tau_2 \sim (c_2/c_1)^3 \sim 10^{-3}$ (c_2 and c_1 are the second and first sound velocities, respectively). In effect, the first sound is in quasi-equilibrium with the second sound waves and induces an effective four-wave mixing for the latter (78). In the turbulent regime that forms at high enough driving forces, both the high-frequency energy E - and low-frequency N -cascades are becoming established, in close similarity with BECs considered above. For this coupled first sound-second sound wave turbulence, the exponents found from the

solution of respective kinetic equations are equal to $\nu_E = -9/2$ and $\nu_{\mathcal{N}} = -4$ (78, 79). It is worth noting that, because of the big difference between the first and second sound velocities, the first and second sound modes with comparable frequencies are only resonantly coupled. In effect, the general kinetic equations for waves can be represented in the form of a differential equation that describes the high-order (hyper) diffusion of both integrals of motion E and \mathcal{N} in k -space (78).

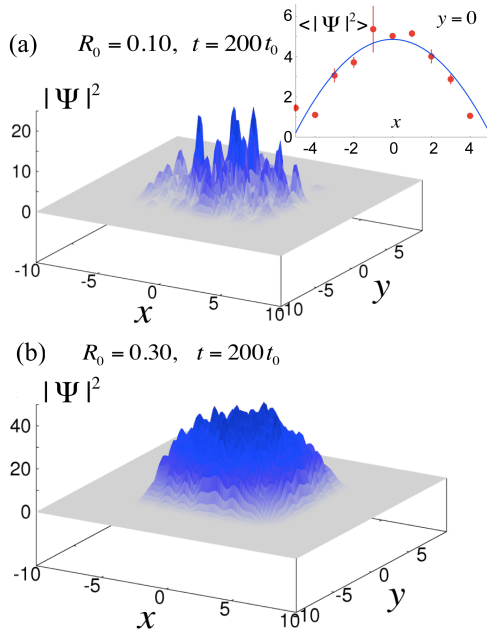


Fig. 4. The exciton density profiles at $t = 200t_0$ for the pumping rates (a) $R_0 = 0.1$ and (b) $R_0 = 0.3$ in a turbulent excitonic BEC. The system is driven in the spectral range of 4th – 6th harmonics. The coordinates are expressed in units of $\ell_0 = 0.9 \mu\text{m}$, and time is expressed in units of $t_0 = 1.6 \text{ ns}$ for the trapping potential strength $\alpha = 50 \text{ eV/cm}^2$. The inset in frame (a) shows the exciton density plotted at $y = 0$ and averaged over the time period $50t_0 < t < 200t_0$ and three independent runs (points). The curve in the inset shows the fitting by the Thomas-Fermi distribution (60). After (15).

Formation of the turbulent spectra after the application of the external driving force is self-similar; however, the character of how the wave distribution approaches the steady state is quite different for the high- and low-frequency spectral domains. Specifically, formation of the high frequency, direct cascade is of the “explosion type” with a finite formation time $\sim \tau_2$. For the inverse cascade, the build-up process requires a time $\sim (k_d L)\tau_2$ that is much longer than is needed for formation of the direct cascade (k_d is the characteristic wave vector of the driving force and L is the system size). In both cases, the transient processes can be understood as the propagation of formation fronts towards high and low frequencies respectively from the driving frequency scale.

Excitonic superfluids in semiconductors. For an excitonic superfluid localized in the (x, y) directions in the trapping potential $V(\mathbf{x})$, the non-equilibrium Gross-Pitaevskii Equation 8 can be solved by expanding the condensate wave function, $\psi(\mathbf{x}, t) = \sum_{\mathbf{n}} A_{\mathbf{n}}(t)\varphi_{\mathbf{n}}(\mathbf{x})$, over the basis functions $\varphi_{\mathbf{n}}(\mathbf{x})$, which are the eigenfunctions of the Hamiltonian for a single quantum particle in a parabolic potential. It is worth noting that the time-dependent spectral amplitudes $A_{\mathbf{n}}(t)$ are similar to the spectral amplitudes $\hat{\psi}_{\mathbf{k}}$ introduced above. However, in contrast to a homogeneous system for which the wave vector \mathbf{k} is well-defined, the single-particle excitation spectrum in the trapping potential is labeled by the two-dimensional integer index $\mathbf{n} = (n_x, n_y)$. In this case, the coupling with the external pumping

is characterized by the matrix elements R_0 of the \hat{R} operator, which is diagonal in the basis $\{\varphi_{\mathbf{n}}(\mathbf{x})\}$. Specifically, to describe the interaction of high-frequency modes with external driving, we take the matrix elements of \hat{R} equal to $R_{\mathbf{n}} = R_0$ if $n_1 < (n_x^2 + n_y^2)^{1/2} \leq n_2$ and $R_{\mathbf{n}} = 0$ otherwise (15). We refer to R_0 as the pumping rate.

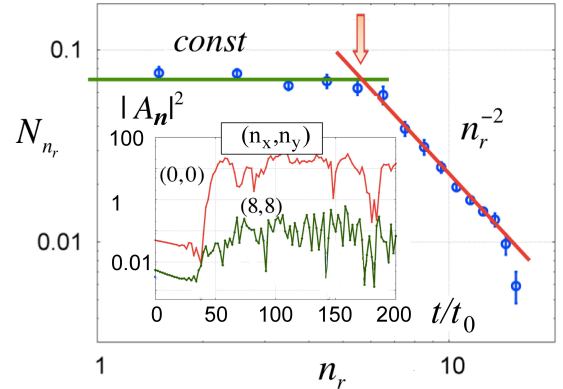


Fig. 5. Angle-averaged occupation number in the excitonic turbulent BEC, N_{n_r} , as a function of the radial spectral number n_r , plotted on a log-log scale. The averaging window for N_{n_r} is $\Delta n = 3$. The center of the pumping region is indicated by the vertical arrow. The lines show a power-law-like distribution for $N_{n_r} = \text{const} \times n_r^\nu$ at $\nu = 0$ and $\nu = -2$. Inset: Time oscillations of the squared spectral amplitudes $|A_{\mathbf{n}}|^2$ at $\mathbf{n} = (0, 0)$ (the fundamental mode) and $(8, 8)$. After (15).

It was observed that, if the exciton condensate is driven by an external laser pumping at high enough spectral modes, the spatial distribution of excitons in the BEC fluctuates strongly, as is demonstrated in Fig. 4. However, the exciton density averaged over a sufficiently long time is given by a smooth function that is well described by the Thomas-Fermi distribution known for the atomic BECs (60) (see inset in Fig. 4(a)). With increasing pumping rate R_0 , the average density of the exciton BEC grows but the density oscillations are sustained as seen in Fig. 4(b).

To better characterize this oscillatory state of the excitonic BEC, we show in Fig. 5 the dependence on time of the squared spectral harmonics, $|A_{\mathbf{n}}(t)|^2$. It is clearly evident that the spectral amplitudes (and hence the occupation of the respective quantum states) oscillate strongly. These latter oscillations correspond to a redistribution of particles between the spectral modes with simultaneous exchange of energy between the modes, in full analogy with the wave-turbulence picture described above. To characterize this excitonic turbulent state more fully, we also plot in Fig. 5 the radial time-averaged occupation number spectrum, $N_{n_r} = \sum_{\mathbf{n}=\mathbf{n}_r}^{\mathbf{n}_r+\Delta\mathbf{n}} \langle |A_{\mathbf{n}}(t)|^2 \rangle$. It is averaged over multiple realizations, over a time window, and also over the window Δn in the spectral space in order to reduce temporal oscillations; $n = (n_x^2 + n_y^2)^{1/2}$ is the radial spectral number. It can be seen that, at spectral numbers lower and higher than the characteristic pumping region (arrowed), power-law-like distributions of occupation number, $N_{n_r} \propto n_r^\nu$, are formed. Specifically, in Fig. 5, the power exponents are $\nu = 0$ and $\nu = -2$ in the low- and high-frequency domains, respectively. These distributions are similar to the Kolmogorov-like turbulent spectra observed in superfluid ^4He (12, 71) and proposed in Refs. (18, 19) in relation to the formation of atomic BECs. Thus, we infer that a turbulent state is formed in the exciton BEC, and that it is characterized by the establishment of particle and energy fluxes through the spectral scales of the system. It is seen in Fig. 5 that the power-like spectra are only formed within one decade of the n_r scale. It is worth noting that the width of such an interval, in which power-like turbulent spectra are realized, varies in a wide range in different systems, from less of one decade (80) to a few decades (12, 81).

Turbulence in an exciton-polariton condensate. Another condensed matter system where turbulence can be formed has recently been discovered in numerical experiments (82, 83) on microcavity polaritons, which are quantum superpositions of excitons and microcavity photons. The physics of polariton BECs is a fast-developing field, and substantial progress has been made during the past decade (we refer the readers to recent reviews (84, 85)). Interest in polariton physics is attributable in part to the promising potential applications in quantum and optical computing (51, 52, 86). In a polariton BEC, a uniform, steady-state condensate becomes unstable due to attractive interactions and mutual scattering between different excitation modes in the condensate (82). The development of the instability results in the formation of turbulent spatial structures that correspond to exciton and photon density modulations in the microcavity. In the existing theory of polariton WT, only the lower, light-like polariton branch of elementary excitations has been taken into account. However, the dynamics is also mediated by interactions with the upper, exciton-like polariton branch as well as with a bath of non-condensed excitons and polaritons (84). Recently it was found in the simulations (87) that interactions with polaritons above the condensate can lead to peculiarities of the ground-state polariton BEC density and, in particular, to the formation of a density minimum at the center of the polariton cloud. The interaction of the BEC with thermal excitations above the condensate are of special interest because of many similarities between atomic condensates at finite temperature and polariton BEC (88). Development of a general polariton WT theory where all the above-mentioned effects are taken into account is a target for future investigations.

4. Conclusion and outlook

In conclusion, wave turbulence provides a unified view of nonlinear transport phenomena in a diversity of different systems including atomic Bose-Einstein condensates, waves in the bulk and on the surface of quantum fluids, and semiconductors. WT manifests itself through formation of the power-law-like, Kolmogorov-Zakharov spectra for the conserved quantities, which are the energy and, under certain conditions, the number of particles (or properly defined “number of waves”). In all these cases, the KZ spectra carry the fluxes of respective quantities from the pumping spectral region, at which the system is driven by an external force, towards the high- or low-frequency domains. The fluxes are eventually absorbed by viscous damping at short wavelength scales or may lead to condensation at long wavelength scales of the order of the system size.

It is worth noting that, in addition to the cases considered above, there is strong numerical evidence for WT formation in a system closely related to semiconductors – the excitonic BEC in two doped graphene layers separated by a semiconductor or insulating barrier

(16). In this case, the binding energy of the charges to graphene is higher than the corresponding energy in semiconductor quantum wells; this results in a longer excitonic lifetime and thus, under some circumstances, in more favorable conditions for Bose-Einstein condensation. However, experimental studies of exciton dynamics in such embedded multi-layered graphene structures have not yet been achieved, in particular because of difficulties in their synthesis.

Another closely related system where WT could potentially be applied is a BEC of light (89). Here, the photon-photon interactions, which are of key importance for formation of a stable BEC, are mediated by optically active particles (dye) added into the medium; these particles absorb and then re-emit light thus providing a channel for the thermalization in the photonic system. Emission of phonons in the medium during photon-dye molecule interactions can result in spatial non-locality of the effective photon-photon scattering. Further development of WT theory will be needed to account for these non-local effects.

Recent experiments have demonstrated the possibility of the Bose-Einstein condensation of magnons, collective excitations that carry spin, in Yttrium-Iron-garnet at room temperature (90). While the possibility of BEC in a magnon system has been discussed during the past ten years (91, 92), and the application of WT to spin systems has been developed in detail in the monograph (93), the approach based on the Gross-Pitaevskii equation for a magnon BEC has only recently been implemented (94), and there is still a large field here for future research.

It is clear that huge progress has been made with the theory of WT but that, as already remarked, the corresponding experimental studies are still in their infancy. If history is a reliable guide, then the advent of additional experimental data may verify some of the theoretical predictions, but there will almost certainly be areas of disagreement and unexpected features requiring further extensions and developments of the theory.

ACKNOWLEDGMENTS. We are grateful for many valuable discussions with colleagues and collaborators including, especially, V.B. Efimov, A.N. Ganshin, L.P. Mezhov-Deglin, A.A. Levchenko, R.Ya. Kezerashvili, O.L. Berman, and Yu.E. Lozovik. G.V.K. gratefully acknowledges support from the PSC CUNY awards #65103-00 43 and # 66140-00 44. P.V.E.McC. is grateful for support under the Materials World Network program of the Engineering and Physical Sciences Research Council (UK) and the US National Science Foundation [EPSRC Grant No. EP/H04762X/1]. S.V.N. gratefully acknowledges support from the government of Russian Federation via grant No. 12.740.11.1430 for supporting research of teams working under supervision of invited scientists. G.V.K. acknowledges the Center for Theoretical Physics at NYC College of Technology for providing computational resources.

- Zakharov VE, L'vov VS, Falkovich G (1992) *Kolmogorov Spectra of Turbulence I* (Springer, Berlin).
- Nazarenko S (2011) *Wave Turbulence* (Springer-Verlag, Heidelberg).
- Brazhnikov MY, Kolmakov GV, Levchenko AA, Mezhov-Deglin LP (2002) Observation of capillary turbulence on the water surface in a wide range of frequencies. *Europhys. Lett.* 58:510–516.
- Cobelli P, et al. (2011) Different regimes for water wave turbulence. *Phys. Rev. Lett.* 107:214503.
- Lukaschuk S, Nazarenko S, McLelland S, Denissenko P (2009) Gravity wave turbulence in wave tanks: space and time statistics. *Phys. Rev. Lett.* 103:044501.
- Dyachenko S, Newell AC, Pushkarev A, Zakharov VE (1992) Optical turbulence – weak turbulence, condensates and collapsing filaments in the nonlinear Schrödinger equation. *Physica D* 57:96–160.
- Bortolozzo U, Laurie J, Nazarenko S, Residori S (2009) Optical wave turbulence and the condensation of light. *J. Opt. Soc. Amer. B – Optical Phys.* 26:2280–2284.
- Gurbatov SN, Kurin VV, Kustov LM, Pronchatov-Rubtsov NV (2005) Physical modeling of nonlinear sound wave propagation in oceanic waveguides of variable depth. *Acoust. Phys.* 51:152–159.
- Ryutova M, Tarbell T (2003) MHD shocks and the origin of the solar transition region. *Phys. Rev. Lett.* 90:191101.
- Bisnovatyi-Kogan GS, Silich SA (1995) Shock-wave propagation in the nonuniform interstellar medium. *Rev. Mod. Phys.* 67:661–712.
- Kolmakov GV, et al. (2004) Quasi-adiabatic decay of capillary turbulence on the charged surface of liquid hydrogen. *Phys. Rev. Lett.* 93:074501.
- Abdurakhimov LV, Brazhnikov MY, Remizov IA, Levchenko AA (2010) Observation of wave energy accumulation in the turbulent spectrum of capillary waves on the He-II surface under harmonic pumping. *JETP Lett* 91:271–276.
- Kolmakov GV, Efimov VB, Ganshin AN, McClintock PVE, Mezhov-Deglin LP (2006) Formation of a direct Kolmogorov-like cascade of second sound waves in He II. *Phys. Rev. Lett.* 97:155301.
- Berman OL, Kezerashvili RY, Kolmakov GV (2011) Introduction to nonlinear phenomena in superfluid liquids and Bose-Einstein condensates: helium, semiconductors and graphene. *Contemp. Phys.* 52:319–340.
- Berman OL, Kezerashvili RY, Kolmakov GV, Lozovik YE (2012) Turbulence in a Bose-Einstein condensate of dipolar excitons in coupled quantum wells. *Phys. Rev. B* 86:045108.
- Berman OL, Kezerashvili RY, Kolmakov GV (2012) On nonlinear dynamics of a dipolar exciton BEC in two-layer graphene. *Phys. Lett. A* 376:3664–3667.
- Henn EAL, Seman JA, Roati G, Magalhaes KMF, Bagnato VS (2009) Emergence of turbulence in an oscillating Bose-Einstein condensate. *Phys. Rev. Lett.* 103:045301.

18. Lvov Y, Nazarenko S, West R (2003) Wave turbulence in Bose-Einstein condensates. *Physica D* 184:333–351.
19. Zakharov VE, Nazarenko SV (2005) Dynamics of the Bose-Einstein condensation. *Physica D* 201:203–211.
20. Proment D, Nazarenko S, Onorato M (2009) Quantum turbulence cascades in the Gross-Pitaevskii model. *Phys. Rev. A* 80:051603.
21. Proment D, Nazarenko S, Onorato M (2012) Sustained turbulence in the three-dimensional Gross-Pitaevskii model. *Physica D* 241:304–314.
22. Kosterlitz JM, Thouless DJ (1973) Ordering, metastability and phase transitions in two-dimensional systems. *J. Phys. C: Solid St. Phys.* 6:1181–1203.
23. Nazarenko S, Onorato M (2006) Wave turbulence and vortices in Bose-Einstein condensation. *Physica D* 219:1–12.
24. Nazarenko S, Onorato M (2007) Freely decaying turbulence and Bose-Einstein condensation in Gross-Pitaevskii model. *J. Low Temp. Phys.* 146:31–46.
25. Vinen WF (2001) Decay of superfluid turbulence at a very low temperature: The radiation of sound from a Kelvin wave on a quantized vortex. *Phys. Rev. B* 64:134520.
26. L'vov VS, Nazarenko S (2010) Spectrum of Kelvin-wave turbulence in superfluids. *JETP Lett.* 91:428–434.
27. Kozik E, Svistunov B (2004) Kelvin-wave cascade and decay of superfluid turbulence. *Phys. Rev. Lett.* 92:035301.
28. Boue L, et al. (2011) Exact solution for the energy spectrum of Kelvin-wave turbulence in superfluids. *Phys. Rev. B* 84:064516.
29. Laurie J, L'vov VS, Nazarenko S, Rudenko O (2010) Interaction of Kelvin waves and nonlocality of energy transfer in superfluids. *Phys. Rev. B* 81:104526.
30. L'vov VS, Nazarenko S (2010) Weak turbulence of Kelvin waves in superfluid He. *Low Temp. Phys.* 36:785–791.
31. L'vov V, Nazarenko S (2010) Comment on "Superfluid turbulence from quantum Kelvin wave to classical Kolmogorov cascades". *Phys. Rev. Lett.* 104:219401.
32. Lebedev VV, L'vov VS, Nazarenko SV (2010) Reply: On role of symmetries in Kelvin wave turbulence. *J. Low Temp. Phys.* 161:606–610.
33. Kozik E, Svistunov B (2010) Geometric symmetries in superfluid vortex dynamics. *Phys. Rev. B* 82:140510(R).
34. Kozik EV, Svistunov BV (2010) Comment on "Symmetries and interaction coefficients of Kelvin waves" (J. Low Temp. Phys. 161, 2010, 548-554 [arXiv:1005.4575]) by Lebedev and L'vov. *J. Low Temp. Phys.* 161:603–605.
35. Kozik EV, Svistunov BV (2009) Theory of decay of superfluid turbulence in the low-temperature limit. *J. Low Temp. Phys.* 156:215–267.
36. L'vov VS, Nazarenko SV, Rudenko O (2008) Gradual eddy-wave crossover in superfluid turbulence. *J. Low Temp. Phys.* 153:140–161.
37. Nazarenko S (2007) Kelvin wave turbulence generated by vortex reconnections. *JETP Lett.* 84:585–587.
38. Boffetta G, Celani A, Dezzani D, Laurie J, Nazarenko S (2009) Modeling Kelvin wave cascades in superfluid helium. *J. Low Temp. Phys.* 156:193–214.
39. Yamamoto Y, Imamoglu A (1999) *Mesoscopic Quantum Optics* (Wiley-Interscience, New York).
40. Snoke DW (2009) *Solid State Physics: Essential Concepts* (Addison-Wesley, San Francisco).
41. Luryi S (1988) Possibility of a direct observation of the time evolution in heterostructure barrier tunneling. *Solid State Communications* 65:787–789.
42. Butov LV, Zrenner A, Abstreiter G, Bohm G, Weimann G (1994) Condensation of indirect excitons in coupled AlAs/GaAs quantum wells. *Phys. Rev. Lett.* 73:304–307.
43. Negoita V, Snoke DW, Eberl K (1999) Harmonic-potential traps for indirect excitons in coupled quantum wells. *Phys. Rev. B* 60:2661–2669.
44. Snoke D (2002) Spontaneous Bose coherence of excitons and polaritons. *Science* 298:1368–1372.
45. Timofeev VB (2005) Collective exciton effects in spatially separated electron – hole layers in semiconductors. *Physics-Uspekhi* 48:295–306.
46. Lozovik YE (2009) Strong correlations and new phases in a system of excitons and polaritons. A polariton laser. *Physics-Uspekhi* 52:286–290.
47. High AA, et al. (2012) Condensation of excitons in a trap. *Nano Lett.* 12:2605–2609.
48. MacDonald AH, Platzman PM, Boebinger GS (1990) Collapse of integer Hall gaps in a double-quantum-well system. *Phys. Rev. Lett.* 65:775–778.
49. Littlewood P (2007) Condensates made of light. *Science* 316:989–990.
50. High AA, Novitskaya EE, Butov LV, Hanson M, Gossard AC (2008) Control of exciton fluxes in an excitonic integrated circuit. *Science* 321:229–231.
51. Johne R, Shelykh IA, Solnyshkov DD, Malpuech G (2010) Polaritonic analogue of Datta and Das spin transistor. *Phys. Rev. B* 81:125327.
52. Amo A, et al. (2010) Exciton-polariton spin switches. *Nat. Photonics* 4:361–366.
53. Schindler C, Zimmermann R (2008) Analysis of the exciton-exciton interaction in semiconductor quantum wells. *Phys. Rev. B* 78:045313.
54. Laikhtman B, Rapaport R (2009) Correlations in a two-dimensional Bose gas with long-range interaction. *Europhys. Lett.* 87:27010.
55. Keeling J, Berloff NG (2008) Spontaneous rotating vortex lattices in a pumped decaying condensate. *Phys. Rev. Lett.* 100:250401.
56. Butov LV, Gossard AC, Chemla DS (2002) Macroscopically ordered state in an exciton system. *Nature* 418:751–754.
57. Zakharov VE, Filonenko NN (1967) Weak turbulence of capillary waves. *J. Appl. Mech. Tech. Phys.* 8:37–40.
58. Falkovich GE, Shafarenko AV (1988) What energy flux is carried away by the Kolmogorov weak turbulence spectrum? *Sov. Phys. JETP* 68:1393–1397.
59. Griffin A, Snoke D, Stringari S, eds. (1995) *Bose-Einstein Condensation* (CUP, Cambridge).
60. Dalforo F, Giorgini S, Pitaevskii L, Stringari S (1999) Theory of Bose-Einstein condensation in trapped gases. *Rev. Mod. Phys.* 71:463–512.
61. Brazhnikov MY, Levchenko AA, Mezhev-Deglin LP (2002) Excitation and detection of nonlinear waves on a charged surface of liquid hydrogen. *Instrum. Expt. Tech.* 45:758–763.
62. Kolmakov GV, et al. (2009) Capillary turbulence on the surface of quantum fluids. In WP Halperin, M Tsubota, eds., *Progress in Low Temperature Physics: Quantum Turbulence*, vol. 16 (Elsevier, Amsterdam), pp. 303–349.
63. Brazhnikov MY, Kolmakov GV, Levchenko AA, Mezhev-Deglin LP (2001) Capillary turbulence at the surface of liquid hydrogen. *JETP Lett.* 73:398–400.
64. Brazhnikov MY, Kolmakov GV, Levchenko AA, Remizov IA, Filatov SV (2001) Measurement of the boundary frequency of the inertial interval of capillary wave turbulence at the surface of liquid hydrogen. *JETP Lett.* 74:583–585.
65. Kolmakov GV, et al. (2005) Decay of the turbulent cascade of capillary waves on the charged surface of liquid hydrogen. *J. Low Temp. Phys.* 138:519–524.
66. Kolmakov GV (2006) Decay of capillary turbulence on the surface of a viscous liquid. *JETP Lett.* 83:58–63.
67. Abdurakhimov LV, Brazhnikov MY, Remizov IA, Levchenko AA (2011) Classical capillary turbulence on the surface of quantum liquid He-II. *Low Temp. Phys.* 37:403–407.
68. Abdurakhimov LV, Brazhnikov MY, Levchenko AA, Remizov IA, Filatov SV (2012) Turbulent capillary cascade near the edge of the inertial range on the surface of a quantum liquid. *JETP Lett.* 95:670–679.
69. Khalatnikov IM (1952) Discontinuities and high-amplitude sound in helium II. *Zh. Eksp. Teor. Fiz.* 23:253–264.
70. Dessler AJ, Fairbank WH (1956) Amplitude dependence of the velocity of second sound. *Phys. Rev.* 104:6–12.
71. Ganshin AN, Efimov VB, Kolmakov GV, Mezhev-Deglin LP, McClintock PVE (2008) Observation of an inverse energy cascade in developed acoustic turbulence in superfluid helium. *Phys. Rev. Lett.* 101:065303.
72. Efimov VB, Ganshin AN, McClintock PVE (2008) Statistical properties of strongly nonlinear waves within a resonator. *Phys. Rev. E* 78:066611.
73. Efimov VB, Ganshin AN, Kolmakov GV, McClintock PVE, Mezhev-Deglin LP (2010) Rogue waves in superfluid helium. *Eur. Phys. J. Special Topics* 185:181–193.
74. Ganshin AN, Efimov VB, Kolmakov GV, Mezhev-Deglin LP, McClintock PVE (2010) Experiments on wave turbulence: the evolution and growth of second sound acoustic turbulence in superfluid ⁴He confirm self-similarity. *New J. Phys.* 12:083047.
75. Efimov VB, Ganshin AN, McClintock PVE (2012) Second-sound acoustic turbulence in superfluid helium: Decay of the direct and inverse energy cascades. *Phys. Rev. B* 86:054515.
76. Efimov VB, Kolmakov GV, Lebedeva EV, Mezhev-Deglin LP, Trusov AB (2000) Generation of second and first sound waves by a pulse heater in He-II under pressure. *J. Low Temp. Phys.* 119:309–322.
77. Rinberg D, Steinberg V (2001) Parametric generation of second sound by first sound in superfluid helium. *Phys. Rev. B* 64:054506.
78. Kolmakov GV (1995) Acoustic turbulence in media with two types of sound. *Physica D* 86:470–479.
79. Pokrovskii VL (1991) Acoustic turbulence. *JETP Lett* 53:583–585.
80. Pushkarev AN, Zakharov VE (1996) Turbulence of capillary waves. *Phys. Rev. Lett.* 76:3320–3323.
81. Falcon C, Falcon E, Bortolozzo U, Fauve S (2009) Capillary wave turbulence on a spherical fluid surface in low gravity. *Europhys. Lett.* 86:14002.
82. Brierley RT, Littlewood PB, Eastham PR (2011) Amplitude-mode dynamics of polariton condensates. *Phys. Rev. Lett.* 107:040401.
83. Berloff NG (2010). Turbulence in exciton-polariton condensates. arXiv:1010.5225 [cond-mat.stat-mech].
84. Deng H, Haug H, Yamamoto Y (2010) Exciton-polariton Bose-Einstein condensation. *Rev. Mod. Phys.* 82:1489–1537.
85. Carusotto I, Ciuti C (2013) Quantum fluids of light. *Rev. Mod. Phys.* 85:299–366.
86. Menon VM, Deych LI, Lisyansky AA (2010) Nonlinear optics: Towards polaritonic logic circuits. *Nature Photonics* 4:345–346.
87. Fernandez YN, Vasilevskiy MI, Trallero-Giner C, Kavokin A (2013) Condensed exciton polaritons in a two-dimensional trap: Elementary excitations and shaping by a gaussian pump beam. *Phys. Rev. B* 87:195441.
88. Proukakis N, Gardiner S, Davis M, Szymanska M, eds. (2013) *Quantum Gases. Finite Temperature and Non-Equilibrium Dynamics*, vol. 1 of *Cold Atoms* (Imperial College Press, London).
89. Klaers J, Schmitt J, Vewinger F, Weitz M (2010) Bose-Einstein condensation of photons in an optical microcavity. *Nature* 468:545–548.
90. Demokritov SO, et al. (2006) Bose-Einstein condensation of quasi-equilibrium magnons at room temperature under pumping. *Nature* 443:430–433.
91. Nikuni T, Oshikawa M, Oosawa A, Tanaka H (2000) Bose-Einstein condensation of dilute magnons in TiCuCl₃. *Phys. Rev. Lett.* 84:5868–5871.
92. Della Torre E, Bennett LH, Watson RE (2005) Extension of the Bloch T^{3/2} law to magnetic nanostructures: Bose-Einstein condensation. *Phys. Rev. Lett.* 94:147210.
93. L'vov VS (1994) *Wave Turbulence under Parametric Excitation. Applications to Magnets* (Springer, Berlin).
94. Nowik-Boltyk P, Dzyapko O, Demidov VE, Berloff NG, Demokritov SO (2012) Spatially non-uniform ground state and quantized vortices in a two-component Bose-Einstein condensate of magnons. *Sci. Reports* 2:482.